Downstream processing from hot-melt extrusion towards tablets: a quality by design approach

W. Grymonpré[a], N. Bostijn[b], S. Van Herck[a], G. Verstraete[a], V. Vanhoorne[a], L. Nuhn[a], P. Rombouts[c], T. De Beer[b], J.P. Remon[a], C. Vervaet[a,*]

[a] Laboratory of Pharmaceutical Technology, Ghent University, Ghent, Belgium
[b] Laboratory of Pharmaceutical Process Analytical Technology, Ghent University, Ghent, Belgium
[c] Department of Electronics and Information Systems (ELIS), Ghent University, Ghent, Belgium

[*]Corresponding author:

C. Vervaet

Ghent University, Laboratory of Pharmaceutical Technology

Ottergemsesteenweg 460

9000 Ghent (Belgium)

Tel.: +32 9 264 80 54

Fax: +32 9 222 82 36

E-mail address: Chris.Vervaet@UGent.be

Abstract

Since the concept of continuous processing is gaining momentum in pharmaceutical manufacturing, a thorough understanding on how process and formulation parameters can impact the critical quality attributes (CQA) of the end product is more than ever required. This study was designed to screen the influence of process parameters and drug load during HME on both extrudate properties and tableting behaviour of an amorphous solid dispersion formulation using a quality-by-design (QbD) approach. A full factorial experimental design with 19 experiments was used to evaluate the effect of several process variables (barrel temperature: 160-200 °C, screw speed: 50-200 rpm, throughput: 0.2-0.5 kg/h) and drug load (0-20%) as formulation parameter on the hot-melt extrusion (HME) process, extrudate and tablet quality of *Soluplus®-Celecoxib* amorphous solid dispersions. A prominent impact of the formulation parameter on the CQA of the extrudates (i.e. solid state properties, moisture content, particle size distribution) and tablets (i.e. tabletability, compactibility, fragmentary behaviour, elastic recovery) was discovered. The resistance of the polymer matrix to thermo-mechanical stress during HME was confirmed throughout the experimental design space. In addition, the suitability of Raman spectroscopy as verification method for the active pharmaceutical ingredient (API) concentration in solid dispersions was evaluated. Incorporation of the Raman spectroscopy data in a PLS model enabled API quantification in the extrudate powders with none of the DOE-experiments resulting in extrudates with a CEL content deviating > 3 % of the label claim. This research paper emphasized that HME is a robust process throughout the experimental design space for obtaining amorphous glassy solutions and for tabletting of such formulations since only minimal impact of the process parameters was detected on the extrudate and tablet properties. However, the quality of extrudates and tablets can be optimized by adjusting specific formulations parameters (e.g. drug load).

Keywords: Hot-melt extrusion (HME), tableting, Quality by Design, solid dispersion, tablet quality, Raman spectroscopy, Principle component analysis (PCA).

1. INTRODUCTION

With the increasing number of new chemical entities being classified as poorly water-soluble, pharmaceutical industry and academia have found themselves a major challenge how to formulate these drug candidates into potent immediate release solid dosage forms. The concept of solubility enhancement through the formation of amorphous solid dispersions has been widely explored for this purpose whereby the drug molecules are dispersed within a solid polymeric matrix. From the broad range of processing techniques which have been used in the last decades for solid dispersion manufacturing (Janssens and Van den Mooter, 2009; Leuner and Dressman, 2000; Paudel et al., 2013; Sethia and Squillante, 2004), hot-melt extrusion (HME) proved extremely suitable since it does not require solvents or water, thereby avoiding potential water-mediated drug degradation or time-consuming drying steps (Saerens et al., 2013). Polymer and API are fed into a heated barrel with screws and the combination of heat, mixing and shear finally results in a homogeneous melt where the drug is preferably molecular dispersed in the polymer matrix (Sarode et al., 2013; Shah et al., 2013). With the efforts made by the pharmaceutical industry to gradually shift the focus from batch towards continuous processing, HME steadily (re-)gained interest since the technique enables superior mixing (both distributive and dispersive) despite the short residence time, allows several downstream options towards various dosage forms and can be run in continuous mode (Plumb, 2005; Saerens et al., 2013; Vervaet et al., 2013). However, there is still insufficient understanding of the critical formulation and process parameters during the HME process of specific pharmaceutical formulations which is reflected in the limited number of pharmaceutical products available on the market processed by HME. Initiated by the Food and Drug Administration (FDA) in order to increase the robustness and quality of a product, pharmaceutical quality-by-design (QbD) was introduced as a strategic product development approach which considers both formulation and process-related factors that affect the critical quality attributes of the final product (Patwardhan et al., 2015). This

already resulted in a few interesting approaches to implement QbD in pharmaceutical melt extrusion processes (Agrawal et al., 2016; Islam et al., 2014; Patwardhan et al., 2015).

In a previous article (Grymonpré et al., 2017), glassy solutions of amorphous polymers with Celecoxib (CEL) were made by HME and further downstream processed via milling and compression into tablets. A polymer platform for HME/tableting purpose was successfully established from which an adequate polymer could be selected. These glassy solutions showed a high milling efficiency and excellent tableting properties, supporting the high potential of HME for implementation in a continuous manufacturing line. In the current research study, a promising polymer-drug combination (using Soluplus® as polymer and Celecoxib as poorly soluble drug) was selected from the platform and subjected to a QbD approach to thoroughly understand how process (barrel temperature, screw speed, throughput) and formulation (drug load) parameters can influence the critical quality attributes of extrudates and tablets prepared from these amorphous solid dispersions.

2. MATERIALS AND METHODS

2.1. Materials

Soluplus® (SOL) was selected for this study as amorphous polymer and kindly donated by BASF (Ludwigshafen, Germany). Celecoxib (CEL, Utag, Amsterdam, The Netherlands), a BCS class II drug, was used as model drug.

2.2. Hot-melt extrusion

HME experiments were performed using a co-rotating, fully intermeshing twin-screw extruder (Prism Eurolab 16, Thermo Fisher, Germany) equipped with a DD Flexwall® gravimetric feeder (Brabender Technology, Germany), two co-rotating twin-screws with 3 mixing zones (length to diameter ratio L/D=25) and a cylindrical die of 3 mm. A data logging system allowed monitoring of the screw torque and barrel well temperature during extrusion. The extrusion barrel is divided into 6 segments which can be heated/cooled separately. Barrel temperature from segment 1 to 5 were set at the same temperature (the actual temperature depended on the experiment as the extrusion temperature was included as a variable in the study), while the die temperature was 140 °C for all experiments to guarantee a solid end product. For each run, 300 g of extrudates were collected at steady state extrusion conditions. After cooling, the extrudates were milled using a knife mill (Moulinex AR110510, France) for 60 s and sieved through a 150 μm sieve.

2.3. Preparation of tablets

Direct compression of the milled extrudates was performed on a rotary tablet press (MODUL™ P, GEA Pharma Systems, Courtoy™, Halle, Belgium) equipped with cylindrical flat-faced Euro B punches of 10 mm diameter and an overfill cam of 16 mm. Tablets of approximately 270 mg were produced at 3 main compaction pressures: 127 (± 9.1), 255 (± 19.2) and 382 (± 27.0) MPa at a turret speed of 5 rpm without using a pre-compression step. Punch deformation at each compaction pressure was calculated and corrected for during this

study. All tablets were analysed for ‘out-of-die’ properties (tablet strength, dimensions and mass) immediately after ejection.

In-die measurements of the compaction properties was performed by linear variable displacement transducers (LVDT) incorporated inside the turret and clamped onto one pair of punches enabling the monitoring of punch stroke movements during a compression cycle (GEA Pharma Systems, Halle, Belgium). Calibration was done prior to each experiment, by interpolating the output voltage of the sensor to physical values during static measurements. A wireless transmission system continuously transmitted the data from these sensors to a data acquisition and analysis system (CDAAS™, GEA Pharma Systems, Halle, Belgium).

2.4. Design of experiments

The experimental ranges for the DOE factors barrel temperature, screw speed, throughput and drug load were determined based on preliminary experiments. A two-level full factorial design with 16 experiments was applied to evaluate the influence of three process parameters: barrel temperature (160-200 °C), screw speed (50-200 rpm), throughput (0.2-0.5 kg/h) and one formulation parameter: drug load (0-20 %) on the HME process and tableting behaviour of the resulting extrudates. Three centerpoint replicates were executed to evaluate the reproducibility. An overview of the experiments is given in Table 1. The responses were regressed against the factors via multiple linear regression (MLR) using MODDE 10.1. software (Umetrics, Umeå, Sweden) where all factors were scaled and centered making the regression coefficients comparable for the different factors. 95% confidence intervals were included for each effect in order to evaluate if factors or factor interactions were significant (i.e. 95% confidence interval of the corresponding effect not including zero).

2.5. Evaluation of the HME process

At each extrusion condition, the torque on the screws was recorded after reaching steady state conditions and the specific mechanical energy (SME) calculated to evaluate the HME process. A reading of 100 % corresponded to the maximum allowable torque of 14.2 Nm.

Prior to each run, the friction torque was determined by running the extruder with screws attached and the barrel empty at the specific conditions as given in Table 1. This friction torque was subtracted from the total recorded torque to obtain the net torque (Godavarti and Karwe, 1997). The SME represents the level of energy per mass unit that is transferred to the material by mechanical input during extrusion (Domenech et al., 2013) and was calculated as follows (Martin, 2013):

$$SME\ (KWh/kg) = (motor\ rating)\ x\ (net\ torque) x\ \frac{N}{Nmax\ x\ throughput}\ x\ gearbox\ efficiency \quad (1)$$

where the extruder had a motor rating of 1.5 KW and a maximum screw speed (N_{max}) of 500 rpm. Net torque (%), operational screw speed (N) and throughput (kg/h) varied based on the experimental settings. Regarding the technical specification of the extruder drive, the gearbox efficiency was set at 0.95.

2.6. Evaluation of extrudates

2.6.1. Thermal analysis

Modulated Differential Scanning Calorimetry (MDSC) measurements were performed both after HME and milling in order to verify the solid state properties of all formulations after each processing step. A heating rate of 2 °C/min and a modulation of 0.318 °C/min over 2 cycles (heat/cool/heat) from -20 to 200 °C was used. The MDSC cell was purged with dry nitrogen at a flow rate of 50 ml/min. Three samples of each experimental run were analysed using the TA instruments Universal Analysis 2000 software.

2.6.2. Particle size analysis

Particle size distribution (PSD) of the powders was recorded (n=3) by laser diffraction (Mastersizer-S long bench, Malvern Instruments, Malvern, UK) via a dry dispersion method in volumetrical distribution mode using a 300 RF lens combined with a dry powder feeder at a feeding rate of 3.0 G and a jet pressure of 2.0 bar (Malvern Instruments, Malvern, UK).

2.6.3. Moisture content

Immediately before tabletting, loss on drying (LOD) was performed (n=3) on the powders corresponding to each experimental run to determine residual moisture content using a Mettler LP16 moisture analyser, including an infrared dryer and a Mettler PM460 balance (Mettler-Toledo, Zaventem, Belgium). Approximately 1 g of sample was dried at 105 °C until the rate of change was less than 0.1% w/w for 30 s.

2.6.4. Flowability

The flow rate of the powders was determined using a flowability testing device (FlowPro, IPAT, Finland) which consists of a frame, sample holder (5.96 ml) with orifice (3.0 mm) and an analytical scale. Vertical oscillations of the sample holder break the cohesive forces in the powder bed and allow the powder to flow through the orifice. The mass discharged from the sample holder is measured over time in order to calculate the flow rate (mg/s) (Sandler et al., 2010). 5% of the mass flow function at the beginning and at the end was not taken into account to minimize the non-linearity of the mass flow (Seppälä et al., 2010). All samples were measured in triplicate.

2.6.5. Size Exclusion Chromatography

Molecular weight distribution analysis was applied to verify if the HME settings used in this experimental design influenced this property of the polymer. Size exclusion chromatography (SEC) measurements were performed on a Shimadzu 20A system using dimethylacetamide (DMAc) supplemented with 50 mM LiBr as mobile phase. The system was equipped with a 20A ISO-pump and a 20A refractive index detector (RID). Measurements were recorded at 50 °C with a flow rate of 0.700 mL/min. Calibration of the 2 PL 5 µm Mixed-D columns was done with poly(methyl methacrylate) (PMMA) standards obtained from PSS (Mainz, Germany). Samples were run with toluene as an internal standard. All formulations of

the experimental design space without CEL (exp. 1-8) were analysed in triplicate together with the neat (non-processed) polymer. In addition, a SOL sample, processed at elevated temperatures (350 °C) to maximize the stress on the polymer, was analysed in order to verify if the technique was able to detect changes in the polymer molecular weight.

2.6.6. Raman spectroscopy

A calibration model was developed allowing off-line API quantification in the extrudates using Raman spectroscopy. Nine different SOL-CEL mixtures, containing 5, 10, 18, 19, 20, 21, 22, 30 and 40 % (w/w) CEL, were extruded at centerpoint-settings (Table 1) and milled to powders. Five validation mixtures of SOL-CEL, containing 19, 20, 21, 25 and 35 % drug were extruded at the same extrusion parameters to evaluate the suitability of Raman spectroscopy for off-line CEL quantification in glassy solutions. A Raman Rxn2 spectrometer (Kaiser Optical Systems, Ann Arbor, MI, USA), equipped with a fibre-optic PhAT-probe was used for collection of the Raman spectra. The laser wavelength was 785 nm and the spectra were recorded with a resolution of 5 cm^{-1}. For all the formulations an exposure time of 5 s with no averaging was used. The analysed spectral region was 665-1655 cm^{-1}, since this region contained all useful drug and polymer information. Data analysis was performed using SIMCA 13.0.3 (Umetrics, Umeå, Sweden). First derivative pre-processing was applied on the collected spectra of all formulations before principal components analysis (PCA) and partial least squares analysis (PLS). At least 6 spectra of each formulation were used to develop the PLS model, regressing the CEL concentrations (Y) versus the corresponding Raman spectra (X). Validation and uncertainty estimation of the quantitative analytical procedure was performed calculating the following parameters (Li et al., 2011; Saerens et al., 2014):

- Root mean square error of prediction:

$$RMSEP = \sqrt{\left(\sum_{i=1}^{I} \frac{(y_i - \hat{y}_i)^2}{I}\right)} \quad (1)$$

where *I* represent the number of samples, y_i and $\hat{y}_i$ the reference and Raman predicted value for sample i, respectively.

- Relative bias:

$$Relative\ Bias\ (\%) = \left(\frac{[\bar{x}_i - \mu]}{\mu}\right) x100 \quad (2)$$

with $\bar{x}_i$ and μ being the average measured API concentration and the true value of the sample, respectively.

- Relative standard deviation:

$$RSD\ (\%) = \left(\frac{[s\ x\ 100]}{\bar{x}_i}\right) \quad (3)$$

where s denotes the standard deviation on the measured API concentrations of repeated samples whereas $\bar{x}_i$ represents the average measured API concentration of those samples.

2.7. Evaluation of the tableting behaviour

2.7.1. Out-of-die tablet properties

Tablet diametral tensile strength was calculated using the equation described by Fell and Newton (1968):

$$Tablet\ Tensile\ Strength\ (\sigma_t) = \frac{2P}{\pi D t} \quad (4)$$

where *P*, *D* and *t* denotes tablet diametral breaking force (N), tablet diameter (mm) and tablet thickness (mm), respectively, which are determined using a hardness tester (Sotax HT10, Basel, Switzerland).

In order to determine the porosity of the compacts following equation is used:

$$Tablet\ Porosity = 1 - \frac{\rho_{app}}{\rho_{true}} \quad (5)$$

where ρ_{app} and ρ_{true} denote the apparent and true density (g/ml), respectively. The latter was measured using helium pycnometry (AccuPyc 1330, Micrometrics, Norcross, USA), while the apparent density was calculated by dividing the tablet mass by the volume of the tablet.

Out-of-die elastic recovery (ER) of the compacts was calculated based on following equation (Armstrong and Haines-Nutt, 1972):

$$ER\ (\%) = \left(\frac{Ta - Tid}{Tid}\right) x100 \quad (6)$$

for which T_{id} represents the minimal tablet thickness (mm) under maximal compression force 'in-die' and T_a is the tablet thickness (mm) measured immediately after ejection.

2.7.2. In-die tablet properties

Energy plots (i.e. force-displacement curves) were recorded during the compression cycles which enabled the calculation of the energy consumption or dissipation at each phase from the area under the curve (Michaut et al., 2010):

$$E = \int F\ dh \quad (7)$$

where F denotes the compression force (kN) and h the punch separation (mm). All energies are normalised by taking the compact mass into account to allow comparison between the different formulations. Resulting energies are used for calculating two specific compaction properties:

- A plasticity factor (PF) which represents the energy of compaction used for plastic deformation and fragmentation:

$$PF\ (\%) = \frac{net\ energy}{total\ energy}\ x\ 100 \quad (8)$$

- In-die elastic recovery (IER) which represents the elasticity of a material:

$$IER\ (\%) = \frac{T_d - T_c}{T_c}\ x\ 100 \quad (9)$$

where T_d and T_c represents the punch separation after decompression and the minimal punch separation during compression, respectively.

All calculations for in-line measuring the compaction properties were done using the **CDAAS™** software (GEA Pharma Systems, Halle, Belgium) on at least 3 compacts for each formulation.

Using the in-die data of the **CDAAS™** system, Heckel analysis was performed on all formulations using the data at a compaction pressure of approximately 65 MPa. The theory of Shapiro-Konopicky-Heckel is based on following equation (Heckel, 1961):

$$ln\ \frac{1}{E} = KP + A \quad (10)$$

where E is the porosity of the powder bed at a compaction pressure P, K is the slope of the linear part of the plot (with the best R^2 fit) and A is the Y intercept with the linear part of the plot. The mean Heckel yield pressures (P_y) are given by the reciprocal values K, while the intercept of both the linear part of the plot (A) and the non-linear part (I) are used to calculate D_a, D_I.

$$D_{a\,(I)} = 1\text{-}\,e^{-A\,(I)} \quad (11)$$

The difference between D_a and D_I denotes D_b, which describes the reduction in volume due to rearrangement of the particles since A is said to reflect low pressure densification by interparticulate motion (Tarlier et al., 2015).

$$D_b = D_a - D_I \quad (12)$$

2.7.3. Multivariate data analysis

Principal component analysis (PCA) was executed on the relevant compaction data in order to classify the different materials according to their compaction behaviour using the multivariate data analysing software SIMCA 13.0.3 (Umetrics, Umeå, Sweden). PCA is a multivariate projection method which extracts and displays the variation in the data set (Pieters et al., 2013). The data were pre-processed by unit variate scaling and centered in order to balance the weight of each variable.

3. RESULTS AND DISCUSSION

3.1. Evaluation of the HME process

Although the torque values strongly varied in function of the experimental parameters, none of them exceeded 55 % of the maximum torque tolerated by the extruder (Table 2). Torque was mainly influenced by barrel temperature and drug load (Fig. 1) since both factors impact the melt viscosity of the formulation. Higher barrel temperatures reduced the melt viscosity of the formulation and therefore less energy input was required to rotate the screws at a predefined screw speed. The latter also occurred when adding CEL to the formulation, since the API can act as a plasticizer when solubilized in the polymer matrix, yielding lower torque values. These findings were confirmed by analyzing rheological data of SOL-CEL formulations as previously reported (Grymonpré et al., 2017).

Calculation of SME values during the HME process has proven its value in previous research as a variable to quantify mixing in an extruder (Sakai and Thommes, 2013), linking the HME process parameters with thermo-mechanical degradation (Wang et al., 2008) or as key descriptor of the influence of processing on the dispersion state (Domenech et al., 2013). Therefore, SME was added in this research as response of the experimental design (Table 2). The impact of process and formulation parameters on the SME levels during HME is represented by the effect plot in Fig. 2. An effect plot displays the change in the response when a factor varies from its low level (-1) to its high level (+1), with all other factors kept constant at their average values. Increasing the screw rotational speed during HME contributed significantly to higher SME-levels, indicating that more mechanical energy is transferred to the material under such conditions. Factors that reduced the torque such as higher barrel temperatures and drug load resulted in lower SME-levels caused by a decrease of the matrix viscosity under such conditions. When more material is fed into the barrel at fixed settings, the same amount of energy must be transferred to a larger amount of material, thereby reducing SME values.

3.2. Evaluation of the extrudates

For the experiments including CEL as model drug, changing the process parameters during HME had no impact on the solid dispersion type. Glassy solutions were obtained at every condition, indicating the suitability of SOL as polymeric carrier for CEL solid dispersions. This is in accordance to previous research where stable amorphous solid dispersions of SOL-CEL were made with drug loads up to 35 % (Grymonpré et al., 2017). In this experimental design, the drug load ranged from 0 to 20 % since preliminary experiments pointed out that higher drug loads decreased the flow properties of the physical mixtures, thereby hampering the ability of including the throughput as factor in the DOE. As throughput was an important process parameter under investigation in this research paper, a consensus was made by lowering the drug load (i.e. formulation parameter), enabling a profound screening design including both process and formulation parameters.

Higher drug loads reduced the glass transition temperature (T_g) of the resulting extrudates, as CEL acted as plasticizer, while the process parameters had no significant impact on solid state properties of the glassy solutions (Fig. 3). Similar conclusion was drawn after analysis of the particle size distribution (PSD) of the milled extrudates: d_{50} and d_{90} values increased for extrudates containing higher drug load (Fig. 3). Due to the drop in T_g, the material was less brittle during milling at room temperature compared to extrudates without CEL. However, these differences had no impact on the flow properties of the milled formulations, enabling further downstream processing such as (continuous) feeding of a rotary tablet press during tableting. Significant impact of drug load and barrel temperature was detected on the moisture content of the milled extrudates (Fig. 4). When formulating glassy solutions with high drug loads, the moisture content decreases significantly when higher extrusion temperatures are used. It has been described in literature that adsorption of water in dense glassy particles occurs mainly at the surface (via weak interactions) due to the absence of pores penetrable to water (Jouppila, 2006). The level of densification during HME might be influenced by the extrusion temperature at higher drug loads, as smaller amorphous clusters or a more extensive

molecular dispersion are created at elevated extrusion temperatures. Density of the extrudates was indeed higher with increasing drug loads and therefore this could explain the observed impact of extrusion temperature on the moisture content at higher drug loads. Although the effects in this study were relatively small (e.g. maximal deviation of 0.4 %) and the impact of moisture content was not reflected in the tableting behaviour of the formulations, it is an important observation since these effects could be more pronounced for other formulations. In general, it could be concluded that drug load had the most significant impact on the extrudates properties, indicating that for this specific formulation the HME process was very robust.

Commonly in literature, little attention is paid to the influence of processing techniques and settings on the polymer matrix, despite the evidence that extrusion can modify the polymer structure (Alexy et al., 2004; Capone et al., 2007). Molecular weight distribution (MWD) analysis of polymers provided insight into possible thermo-mechanical degradation of SOL during by the HME-process. MWD of extrudates resulting from runs with high, low and medium SME-values (exp. 3, 2 and 4, respectively), which represent the thermo-mechanical energy input during the extrusion process (Wang et al., 2008), were plotted against MWD of non-processed and deliberately stressed SOL in Fig. 5. The method used was able to detect changes in the MWD of SOL based on the peak broadening of the 'stressed' samples towards low and high molecular weight species. It is hypothesized that heat-induced side chain hydrolysis and cross-linking caused these changes in the 'stressed' SOL sample. However, no significant changes in MWD of SOL were detected under the conditions employed in the experimental design space. These findings confirmed the resistance of SOL towards thermo-mechanical stress during HME at regular extrusion settings.

In order to quantify the concentration of CEL in the extrudates, off-line Raman spectroscopy was applied on powders of the formulations containing API (exp. 9-19, Table 1). MDSC and XRD measurements confirmed the absence of crystalline CEL in each formulation, indicating the formation of glassy solutions comparable to the DOE-formulations. The concentration variations are clearly visible in the collected Raman spectra (Fig. 6, above) which is reflected in the PCA scores plot of the collected spectra (Fig. 6, lower). The two principle

components covered nearly all spectral variation, where the first principal component (PC_1) accounted for 96 % of the total variation. It was confirmed from the scores plot that PC_1 captured the spectral variation caused by differences in API-polymer concentration since a clear distinction can be made between the Raman spectra of the calibration set.

A PLS model was developed which allowed prediction of the CEL concentration in the extrudate powders of the DOE-formulations by regressing the off-line collected spectra (X) of the calibration set versus the known CEL concentrations (Y). Two PLS components were sufficient since the goodness of prediction of the model (Q^2=0.996) did not significantly increase when adding extra components. The predictive performance of the PLS model was validated by projecting the Raman spectra of a validation set onto the model in order to predict the corresponding CEL concentrations (Fig. 7). This resulted in a root mean square error of prediction (RMSEP) of 1.84 %. For each validation concentration level, accuracy was evaluated by calculating the trueness and precision (Table 3). A good precision of the method was noticed as the accuracy of all validated concentrations remained within the acceptance limits of 10 % (Saerens et al., 2014). The latter PLS model enabled quantification of CEL (%) in the extrudate powders of correlating experiments of the experimental design (Table 4). None of the experiments in the DOE resulted in extrudates with a CEL content deviating > 3 % of the label claim, taking into account the RMSEP.

3.3. Influence of the design variables on the tableting behaviour

3.3.1. Out-of-die tablet properties

Tabletability was clearly affected by the drug load as can be seen in Fig. 8 (full vs. dotted lines), while changing the process parameters had no significant impact on this tablet property. Tablets manufactured from extrudates formulated with CEL yielded significantly

higher tensile strengths. Additionally, the shape of the curves was influenced by the formulation parameter as the tabletability of formulations without drug was independent of the compaction pressure, while CEL-containing formulations showed an inflection point prior to reaching the 'plateau' phase at higher main compaction pressures. The latter indicated that changes in the mechanical properties of these formulations had occurred, which resulted in tablets of higher tensile strength.

Some of the provided energy during compaction can be stored by materials as elastic energy, which is linked to the elastic recovery during decompression thereby causing disruption of some of the previously formed interparticulate bondings (Sun and Grant, 2001). Fig. 9 represents how process and formulation parameters influence the magnitude of this out-of-die descriptor, with an inverse correlation between drug load and out-of-die elastic recovery. Low values of the latter are preferred, since the phenomenon of capping was linked to modifications in the compact during the decompression phase (Wu et al., 2008) and low out-of-die elastic recoveries are beneficial within the context of continuous tablet coating after ejection.

3.3.2. In-die tableting properties

Previously, we have highlighted the added value of including in-die compaction properties to comprehensively investigate the tableting behaviour of materials since this provided better insight in the compression mechanisms which enable the formation of strong compacts. The compaction properties plasticity factor (PF) and in-die elastic recovery (IER), calculated from the recorded energy plots during a compression cycle, represent the contribution of respectively plastic deformation and elastic behaviour to the tensile strength of a tablet. Drug load had a significant impact on the plastic deformation of the formulation, with higher PF at increasing drug loads, while IER was unaffected by this formulation parameter. Analysis of the Heckel plots allowed to interpret the volume reduction processes during the compression phase, where high P_y and D_b values are indicative for materials undergoing more

particle rearrangement in the low pressure region (Tarlier et al., 2015). Formulation of glassy solutions with increasing levels of CEL yielded higher P_y and D_b values, highlighting the more fragmentary behaviour of these formulations which contributed to their higher tablet tensile strengths (Fig. 8).

3.3.3. Multivariate data analysis

The influence of the design variables on the tableting behaviour was summarized using principle component analysis (PCA) where different compaction properties and mechanical properties were included in order to classify formulations of the different experiments according to the contributions of these individual properties. The two principal components in the PCA accounted for 82.5 % of the total variance in the dataset, the first principal component (PC_1) comprising 68.5 % of the variance. When analysing the PCA bi-plot (Fig. 10) along PC_1, the prominent influence of the formulation parameter drug load stands out with a cluster of the 20 % CEL formulations having low PC1 values (blue triangles), formulations without drug having high PC1 values (orange boxes) and the centerpoint formulations with 10 % CEL having intermediate values (green circles). The loadings indicated that PC_1 (i.e. the direction of the x-axis) differentiated between formulations which experienced more fragmentation and plastic deformation and therefore yielded tablets of higher tensile strength (left of the origin), while it was anti-correlated with the out-of-die elastic recovery (right of the origin). PC_2 (i.e. the direction of the y-axis) captured the flow properties of the powders and the IER which was anti-correlated to the PF.

4. CONCLUSIONS

A QbD approach for HME/tableting was successfully implemented in this research study to evaluate the influence of process parameters and drug load during HME on both extrudate properties and tableting behaviour of an amorphous solid dispersion formulation.

Modulation of the torque was possible by adjustment of the barrel temperature and drug load. Additional variations in screw speed and throughput led to different SME-levels, which represent the input of mechanical energy into the material during HME. Drug load had the most significant impact on the extrudate properties with minimal influence of the process variables. Similar results were obtained when evaluating the tableting behaviour of the formulations with a prominent influence of the formulation parameter (i.e. drug load) on the compaction and mechanical properties and no effect of varying HME process parameters. Increasing drug loads resulted in compacts with higher tensile strength since the volume reduction mechanisms changed towards more fragmentary behaviour combined with more plastic deformation and less out-of-die elastic recovery. A PLS model was developed and validated for Raman spectroscopy data which allowed off-line CEL quantification in the extrudates. This research emphasized that HME is a robust process throughout the experimental design space for obtaining amorphous glassy solutions and tablets of such formulations since only minimal impact was detected of the process parameters on the extrudate and tablet properties. However, the quality of extrudates and tablets can be optimized by adjusting specific formulations parameters (e.g. drug load).

Acknowledgements

The authors would like to thank Camille Vanhoutte for the experimental help and GEA Pharma Systems™ for providing the complementary tooling for measuring punch displacement on the rotary tablet press.

5. LITERATURE

Agrawal, A., Dudhedia, M., Deng, W., Shepard, K., Zhong, L., Povilaitis, E., Zimny, E., 2016. Development of Tablet Formulation of Amorphous Solid Dispersions Prepared by Hot Melt Extrusion Using Quality by Design Approach. AAPS PharmSciTech 17, 214–232.

Alexy, P., Lacik, I., Simkova, B., Bakos, D., Pronayova, N., Liptaj, T., Hanzelova, S., Varosova, M., 2004. Effect of melt processing on thermo-mechanical degradation of poly(vinyl alcohol)s. Polym. Degrad. Stab. 85, 823–830.

Armstrong, N.A., Haines-Nutt, R.F., 1972. Elastic recovery and surface area changes in compacted powder systems. J. Pharm. Pharmacol. 24, Suppl:135P-136.

551 Capone, C., Landro, L. Di, Inzoli, F., Penco, M., Sartore, L., Vinci, L., 2007. Thermal and
552 Mechanical Degradation During Polymer Extrusion Processing. Polym. Eng. Sci. 1813–
553 1819.
554 Domenech, T., Peuvrel-disdier, E., Vergnes, B., 2013. The importance of specific mechanical
555 energy during twin screw extrusion of organoclay based polypropylene nanocomposites.
556 Compos. Sci. Technol. 75, 7–14.
557 Godavarti, S., Karwe, M. V, 1997. Determination of Specific Mechanical Energy Distribution
558 on a Twin-Screw Extruder. J. Agric. Engng Res 67, 277–287.
559 Grymonpré, W., Verstraete, G., Bockstal, P.J. Van, Renterghem, J. Van, Rombouts, P.,
560 2017. In-line monitoring of compaction properties on a rotary tablet press during tablet
561 manufacturing of hot-melt extruded amorphous solid dispersions. Int. J. Pharm. 517,
562 348–358.
563 Heckel, R.W., 1961. An analysis of powder compaction phenomena. Trans. Met. Soc. AIME
564 1001–1008.
565 Islam, M.T., Maniruzzaman, M., Halsey, S.A., Chowdhry, B.Z., 2014. Development of
566 sustained-release formulations processed by hot-melt extrusion by using a quality-by-
567 design approach. Drug Deliv. Transl.Res. 4, 377–387.
568 Janssens, S., Van den Mooter, G., 2009. Review: physical chemistry of solid dispersions. J.
569 Pharm. Pharmacol. 61, 1571–1586.
570 Jouppila, K., 2006. Mono- and Disaccharides: Selected Physicochemical and Functional
571 Aspects, in: Eliasson, A.-C. (Ed.), Carbohydrates in Food. Taylor&Francis Group, pp.
572 41–88.
573 Leuner, C., Dressman, J., 2000. Improving drug solubility for oral delivery using solid
574 dispersions. Eur. J. Pharm. Biopharm. 50, 47–60.
575 Li, Y., Du, G., Cai, W., Shao, X., Al, E.T., 2011. Classification and Quantitative Analysis of
576 Azithromycin Tablets by Raman Spectroscopy and Chemometrics. Am. J. Anal. Chem.
577 2, 135–141.
578 Martin, C., 2013. Twin Screw Extrusion for Pharmaceutical Processes, in: Repka, M.A. (Ed.),
579 Melt Extrusion. pp. 47–79.
580 Michaut, F., Busignies, V., Fouquereau, C., Huet De Barochez, B., Leclerc, B., Tchoreloff, P.,
581 2010. Evaluation of a Rotary Tablet Press Simulator as a Tool for the Characterization
582 of Compaction Properties of Pharmaceutical Products. J. Pharm. Sci. 99, 2874–2885.
583 Patwardhan, K., Asgarzadeh, F., Dassinger, T., Albers, J., Repka, M.A., 2015. A quality by
584 design approach to understand formulation and process variability in pharmaceutical
585 melt. J. Pharm. Pharmacol. 67, 673–684.
586 Paudel, A., Worku, Z.A., Meeus, J., Guns, S., Van Den Mooter, G., 2013. Manufacturing of
587 solid dispersions of poorly water soluble drugs by spray drying: Formulation and
588 process considerations. Int. J. Pharm. 453, 253–284.
589 Pieters, S., Vander Heyden, Y., Roger, J.-M., DHondt, M., Hansen, L., Palagos, B., De
590 Spiegeleer, B., Remon, J.-P., Vervaet, C., De Beer, T., 2013. Raman spectroscopy and
591 multivariate analysis for the rapid discrimination between native-like and non-native
592 states in freeze-dried protein formulations. Eur. J. Pharm. Biopharm. 85, 263–271.
593 Plumb, K., 2005. Continuous Processing in the pharmaceutical industry: Changing the mind
594 set. Chem. Eng. Res. Desing 83, 730–738.
595
596 Saerens, L., Segher, N., Vervaet, C., Remon, J.P., Beer, T. De, 2014. Validation of an in-line
597 Raman spectroscopic method for continuous active pharmaceutical ingredient
598 quantification during pharmaceutical hot-melt extrusion. Anal. Chim. Acta 806, 180–187.
599 Saerens, L., Vervaet, C., Paul, J., Beer, T. De, 2013. Process monitoring and visualization
600 solutions for hot-melt extrusion : a review. J. Pharm. Pharmacol. 66, 180–203.
601 Sakai, T., Thommes, M., 2013. Investigation into mixing capability and solid dispersion
602 preparation using the DSM Xplore Pharma Micro Extruder. J. Pharm. Pharmacol. 66,
603 218–231.
604 Sandler, N., Reiche, K., Heinämäki, J., Yliruusi, J., 2010. Effect of Moisture on Powder Flow
605 Properties of Theophylline. Pharmaceutics 2, 275–290.

606 Sarode, A.L., Sandhu, H., Shah, N., Malick, W., Zia, H., 2013. Hot melt extrusion (HME) for
607 amorphous solid dispersions : Predictive tools for processing and impact of drug-
608 polymer interactions on supersaturation. Eur. J. Pharm. Sci. 48, 371–384.
609 Seppälä, K., Heinämäki, J., Hatara, J., Seppälä, L., Yliruusi, J., 2010. Development of a New
610 Method to Get a Reliable Powder Flow Characteristics Using Only 1 to 2 g of Powder.
611 AAPS PharmSciTech 11, 402–408.
612 Sethia, S., Squillante, E., 2004. Solid dispersion of carbamazepine in PVP K30 by
613 conventional solvent evaporation and supercritical methods. Int. J. Pharm. 272, 1–10.
614 Shah, S., Maddineni, S., Lu, J., Repka, M.A., 2013. Melt extrusion with poorly soluble drugs.
615 Int. J. Pharm. 453, 233–252.
616 Sun, C., Grant, D.J.W., 2001. Influence of crystal structure on the tableting properties of
617 sulfamerazine polymorphs. Pharm. Res. 18, 274–280.
618 Tarlier, N., Soulairol, I., Bataille, B., Baylac, G., Ravel, P., Nofrerias, I., Lefèvre, P., Sharkawi,
619 T., 2015. Compaction behavior and deformation mechanism of directly compressible
620 textured mannitol in a rotary tablet press simulator. Int. J. Pharm. 495, 410–419.
621 Vervaet, C., Vercruysse, J., Remon, J.P., De Beer, T., Vervaet, C., 2013. Continuous
622 Processing of Pharmaceuticals, in: Encyclopedia of Pharmaceutical Science and
623 Technology. Taylor&Francis Group, pp. 644–655.
624 Wang, Y., Steinhoff, B., Brinkmann, C., Alig, I., 2008. In-line monitoring of the thermal
625 degradation of poly (L -lactic acid) during melt extrusion by UV-vis spectroscopy.
626 Polymer (Guildf). 49, 1257–1265.
627 Wu, C., Hancock, B.C., Mills, A., Bentham, A.C., Best, S.M., Elliott, J.A., 2008. Numerical
628 and experimental investigation of capping mechanisms during pharmaceutical tablet
629 compaction. Powder Technol. 181, 121–129.
630
631
632

633
634
635
636
637
638

Figure 1. Contour plot of torque as function of barrel temperature (°C) and drug load (%).

Figure 2. Effect plot of SME including 95% confidence intervals for screw speed (Scr), barrel temperature (T), throughput (Thr) and drug load (Dru) with their interactions (*) as factors.

Figure 3. Effect plots of extrudate properties including 95% confidence intervals: responses T_g (upper figure) and d_{90} (lower figure) for screw speed (Scr), barrel temperature (T), throughput (Thr) and drug load (Dru) with their interactions (*) as factors.

Figure 4. Effect plot including 95% confidence intervals of the moisture content (upper figure) for screw speed (Scr), barrel temperature (T), throughput (Thr) and drug load (Dru) with their interactions (*) as factors while the interaction plot (lower figure) is highlighting the combined effect of barrel temperature (T) and drug load on the moisture content.

Figure 5. Molecular weight distributions (left) of SOL-samples: non-processed (neat), hot-melt extruded at stress condiditions (stressed) or hot-melt extruded using different (low, medium and high) SME conditions (EX). The molecular structure of SOL is shown (right).

Figure 6. Off-line collected Raman spectra with first derivative pre-processing (upper figure) and the corresponding PC1 versus PC2 scores plot (lower figure) of the calibration set for milled extrudates containing 5 % CEL (black), 10 % CEL (red), 20 % CEL (blue), 30 % CEL (yellow) and 40 % CEL (green).

Figure 7. Predicted versus observed CEL concentrations of the Raman spectra of the validation set containing 19 % CEL (black squares), 20 % CEL (red circles), 21 % CEL (blue triangles), 25 % CEL (yellow inverse triangles) and 35 % CEL (green diamond).

Figure 8. Tabletability plot of all experiments (left) and the effect plot including 95% confidence intervals of the tablet tensile strength at 255 MPa (right). Formulations without API (experiments 1-8) are represented by dotted lines (·····), formulations with 20 % drug load (experiments 9-16) are represented by full lines (——) while the centerpoints containing 10 % drug load (experiments 17-19) are displayed by dashed lines (-----).

Figure 9. Out-of-die elastic recovery in function of main compaction pressure for all experiments (left) and the corresponding effect plot including 95% confidence intervals at 255 MPa (right). Formulations without API (experiments 1-8) are represented by dotted lines (·····), formulations with 20 % drug load (experiments 9-16) are represented by full lines (——) while the centerpoints containing 10 % drug load (experiments 17-19) are displayed by dashed lines (-----).

Figure 10. PC_1 vs. PC_2 bi-plot of the determined compaction and flow properties for formulations of experiments containing 20 % CEL (blue triangles), formulations of experiments without drug load (orange boxes) and centerpoints containing 10 % CEL (green circles) for which the number represents the corresponding experiment number in the experimental design. The loadings (red star shape) represent the fragmentation factor (D_b), the heckel value (P_y), the plasticity factor (PF) and the anti-correlated in-die elastic recovery (IER), tablet tensile strength (TS) and out-of-die elastic recovery (AR) for three compaction pressures (low, medium, high) and the flow rate of the powder formulations.

Figure 1. Contour plot of torque as function of barrel temperature (°C) and drug load (%).

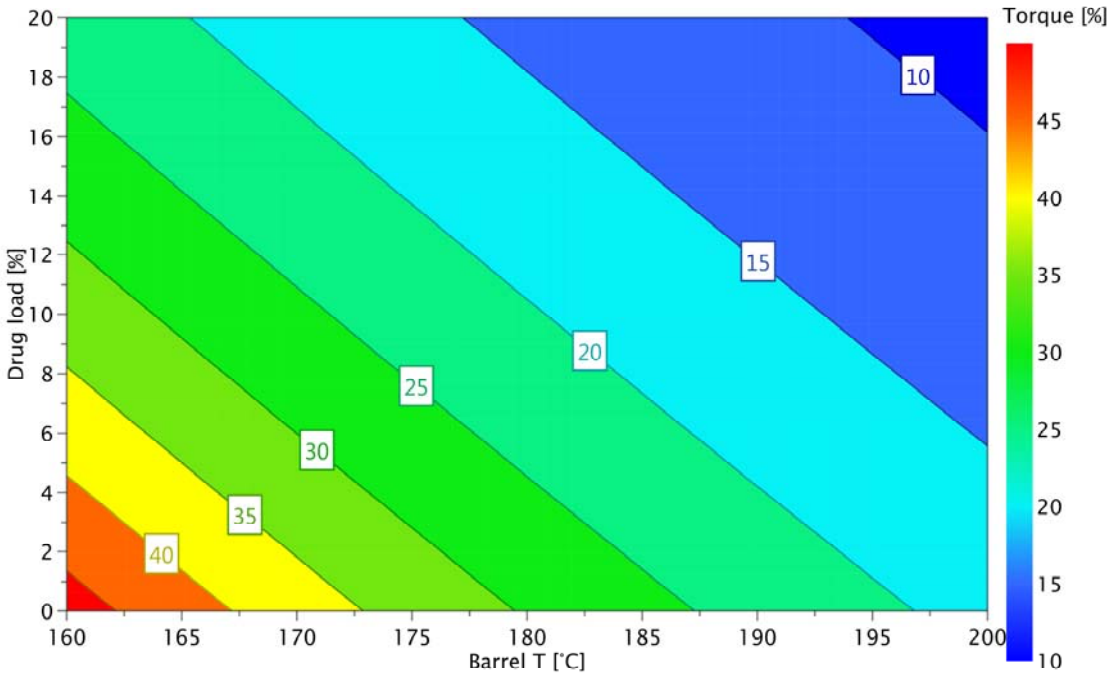

Figure 2. Effect plot of SME including 95% confidence intervals for screw speed (Scr), barrel temperature (T), throughput (Thr) and drug load (Dru) with their interactions (*) as factors.

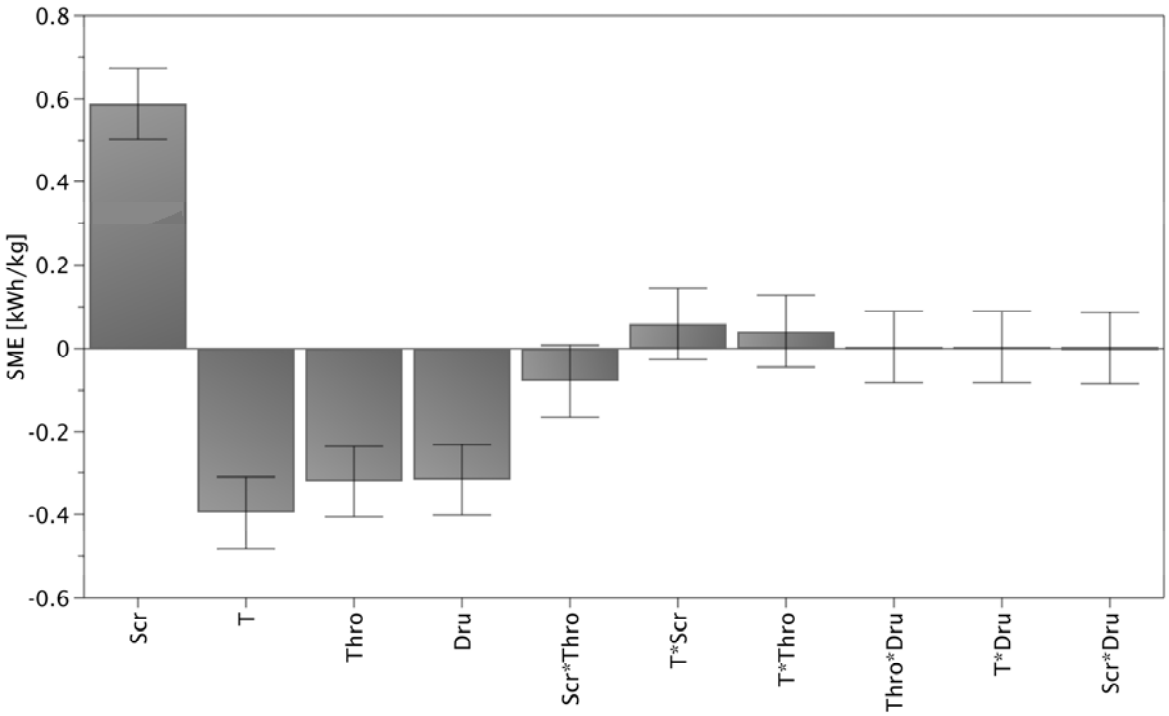

Figure 3. Effect plots of extrudate properties including 95% confidence intervals: responses T_g (upper figure) and d_{90} (lower figure) for screw speed (Scr), barrel temperature (T), throughput (Thr) and drug load (Dru) with their interactions (*) as factors.

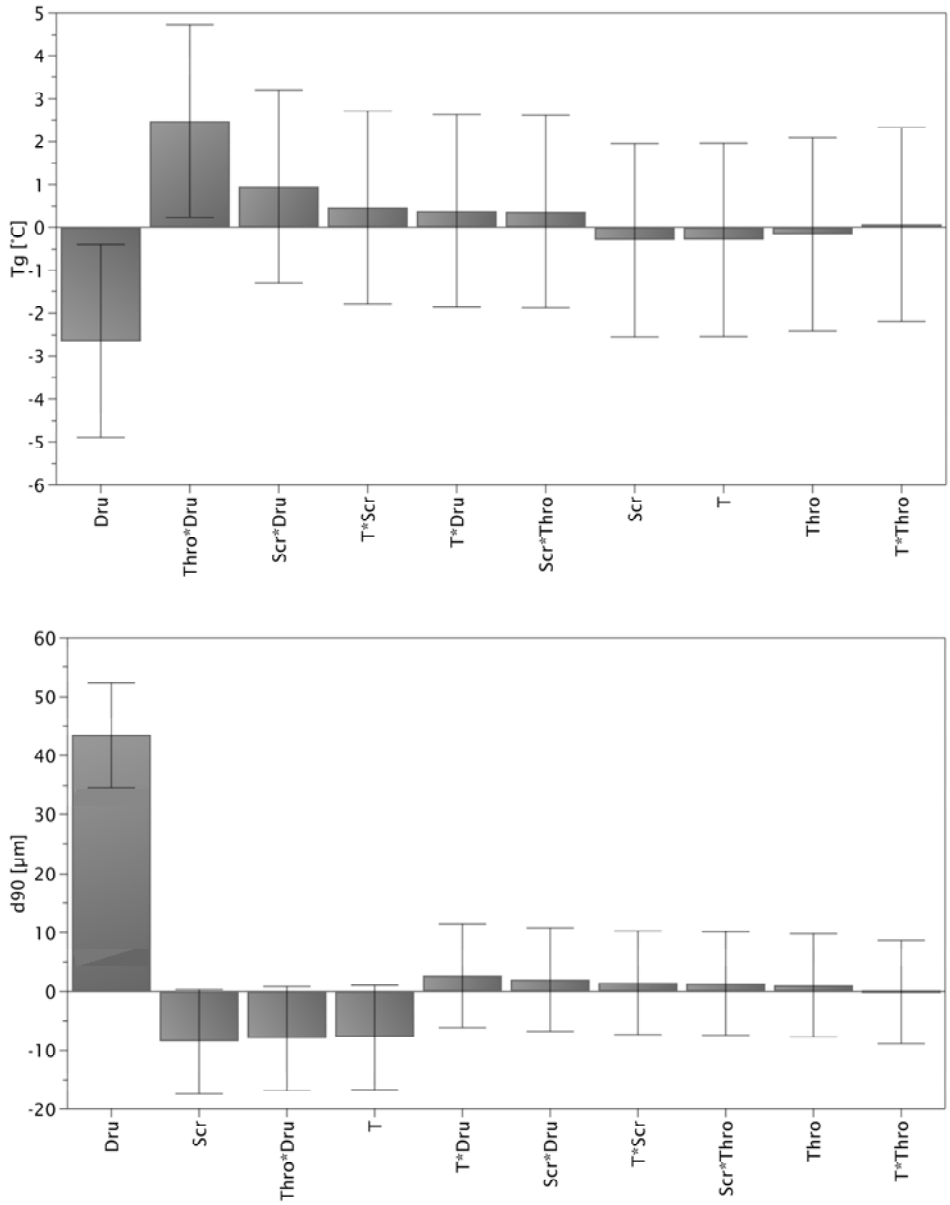

Figure 4. Effect plot including 95% confidence intervals of the moisture content (upper figure) for screw speed (Scr), barrel temperature (T), throughput (Thr) and drug load (Dru) with their interactions (*) as factors while the interaction plot (lower figure) is highlighting the combined effect of barrel temperature (T) and drug load on the moisture content.

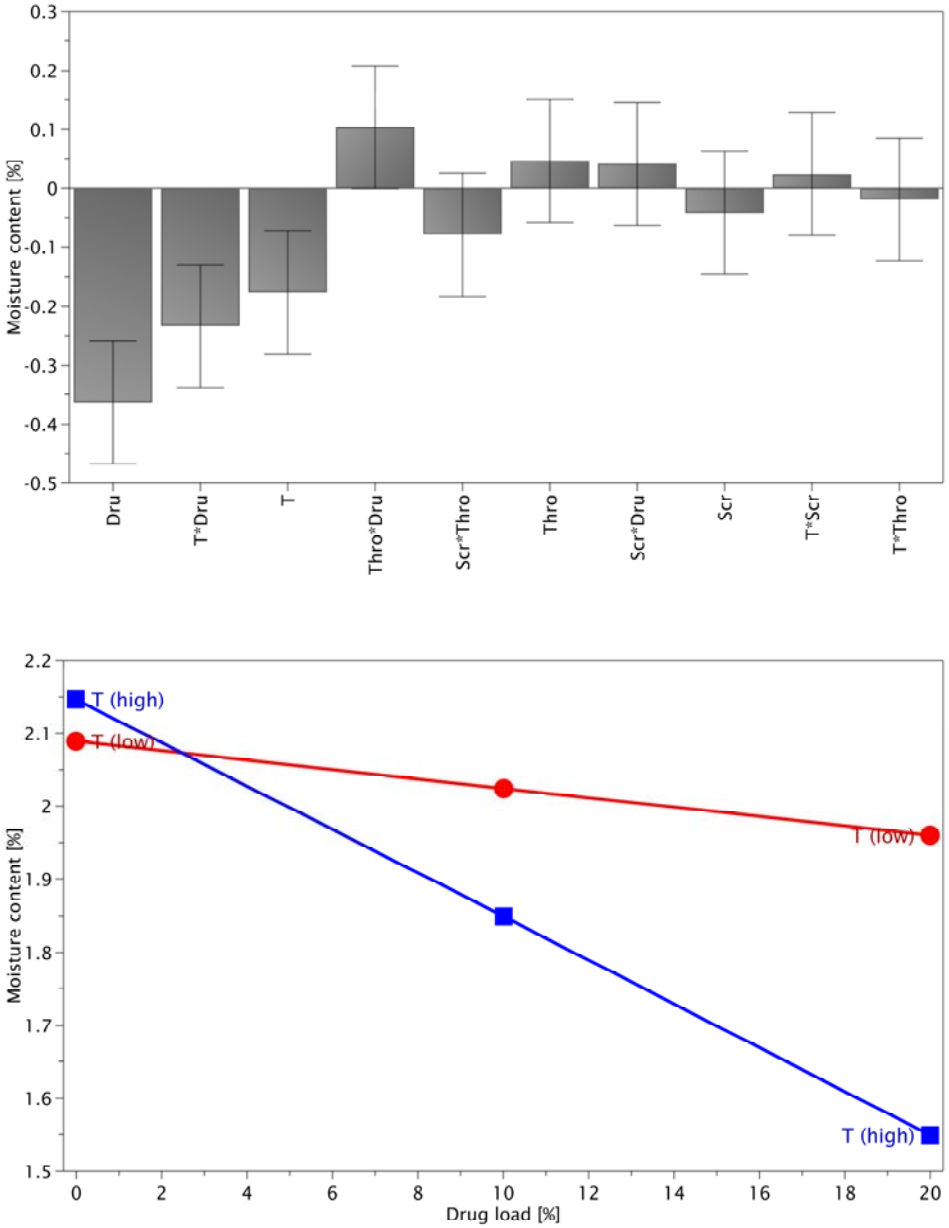

Figure 5. Molecular weight distributions (left) of SOL-samples: non-processed (neat), hot-melt extruded at stress conditions (stressed) or hot-melt extruded using different (low, medium and high) SME conditions (EX). The molecular structure of SOL is shown (right).

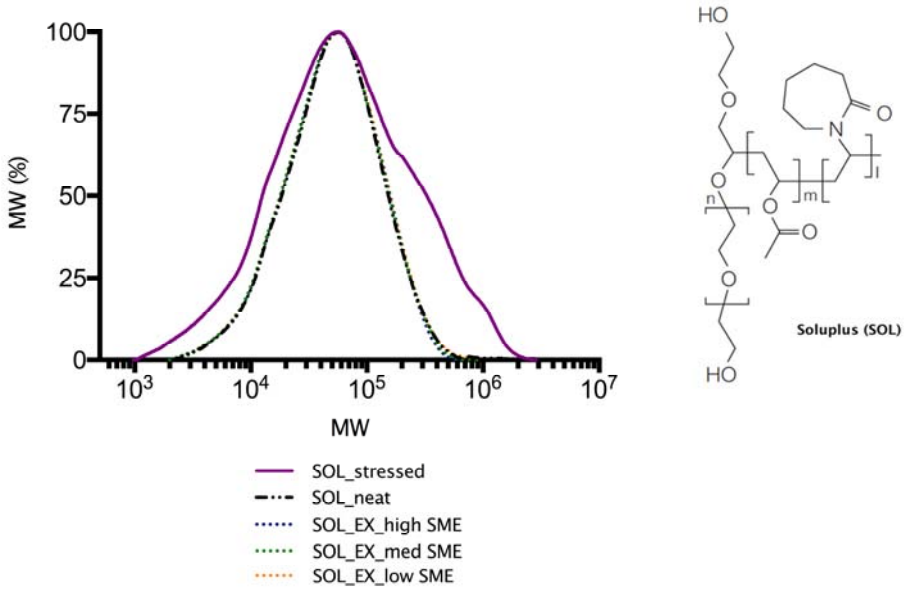

Figure 6. Off-line collected Raman spectra with first derivative pre-processing (upper figure) and the corresponding PC1 versus PC2 scores plot (lower figure) of the calibration set for milled extrudates containing 5 % CEL (black), 10 % CEL (red), 20 % CEL (blue), 30 % CEL (yellow) and 40 % CEL (green).

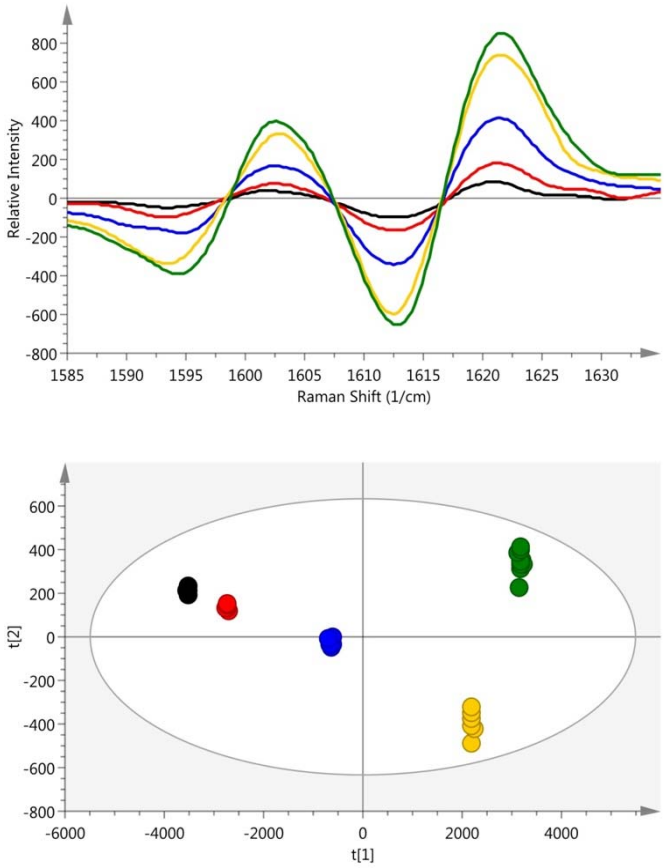

Figure 7. Predicted versus observed CEL concentrations of the Raman spectra of the validation set containing 19 % CEL (black squares), 20 % CEL (red circles), 21 % CEL (blue triangles), 25 % CEL (yellow inverse triangles) and 35 % CEL (green diamond).

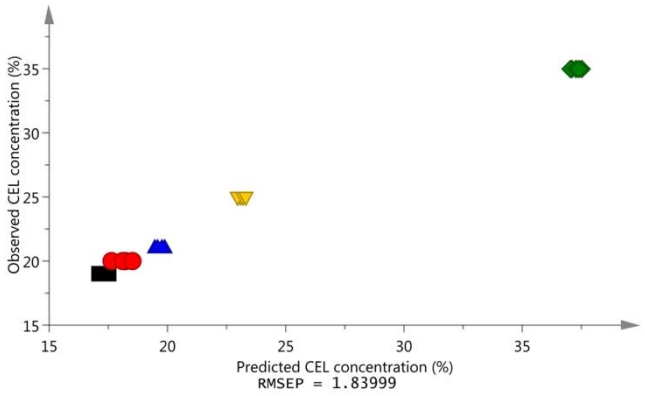

Figure 8. Tabletability plot of all experiments (left) and the effect plot including 95% confidence intervals of the tablet tensile strength at 255 MPa (right). Formulations without API (experiments 1-8) are represented by dotted lines (·····), formulations with 20 % drug load (experiments 9-16) are represented by full lines (——) while the centerpoints containing 10 % drug load (experiments 17-19) are displayed by dashed lines (-----).

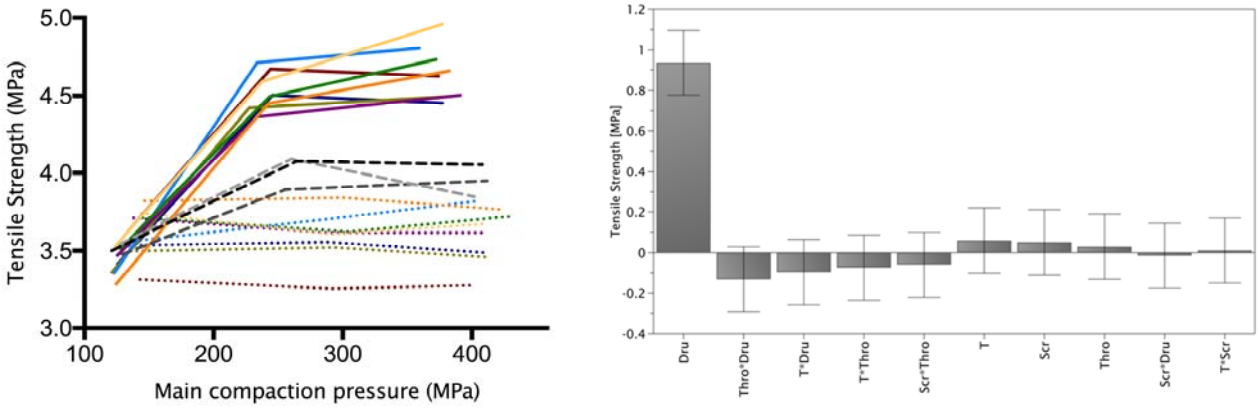

Figure 9. Out-of-die elastic recovery in function of main compaction pressure for all experiments (left) and the corresponding effect plot including 95% confidence intervals at 255 MPa (right). Formulations without API (experiments 1-8) are represented by dotted lines (·····), formulations with 20 % drug load (experiments 9-16) are represented by full lines (——) while the centerpoints containing 10 % drug load (experiments 17-19) are displayed by dashed lines (-----).

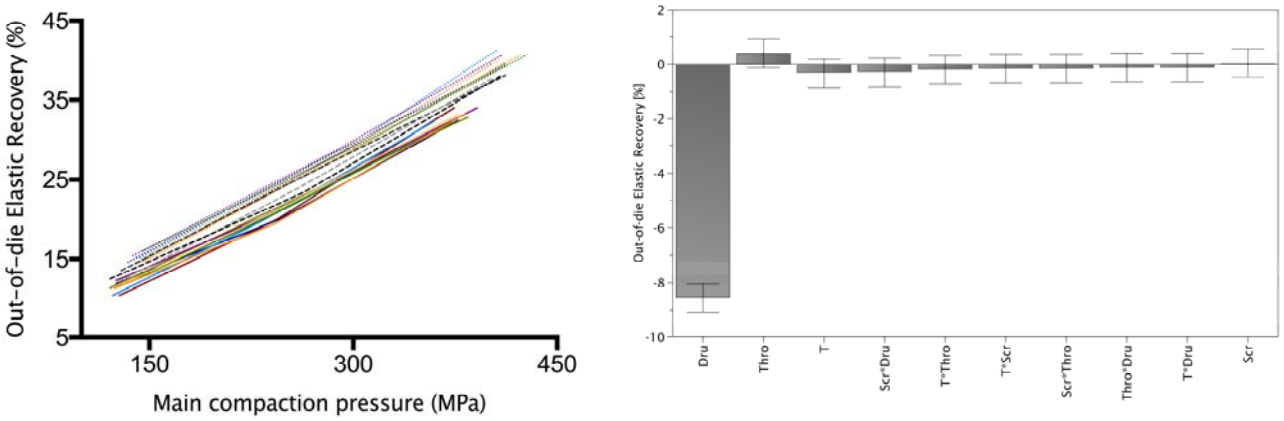

Figure 10. PC_1 vs. PC_2 bi-plot of the determined compaction and flow properties for formulations of experiments containing 20 % CEL (blue triangles), formulations of experiments without drug load (orange boxes) and centerpoints containing 10 % CEL (green circles) for which the number represents the corresponding experiment number in the experimental design. The loadings (red star shape) represent the fragmentation factor (D_b), the heckel value (P_y), the plasticity factor (PF) and the anti-correlated in-die elastic recovery (IER), tablet tensile strength (TS) and out-of-die elastic recovery (AR) for three compaction pressures (low, medium, high) and the flow rate of the powder formulations.

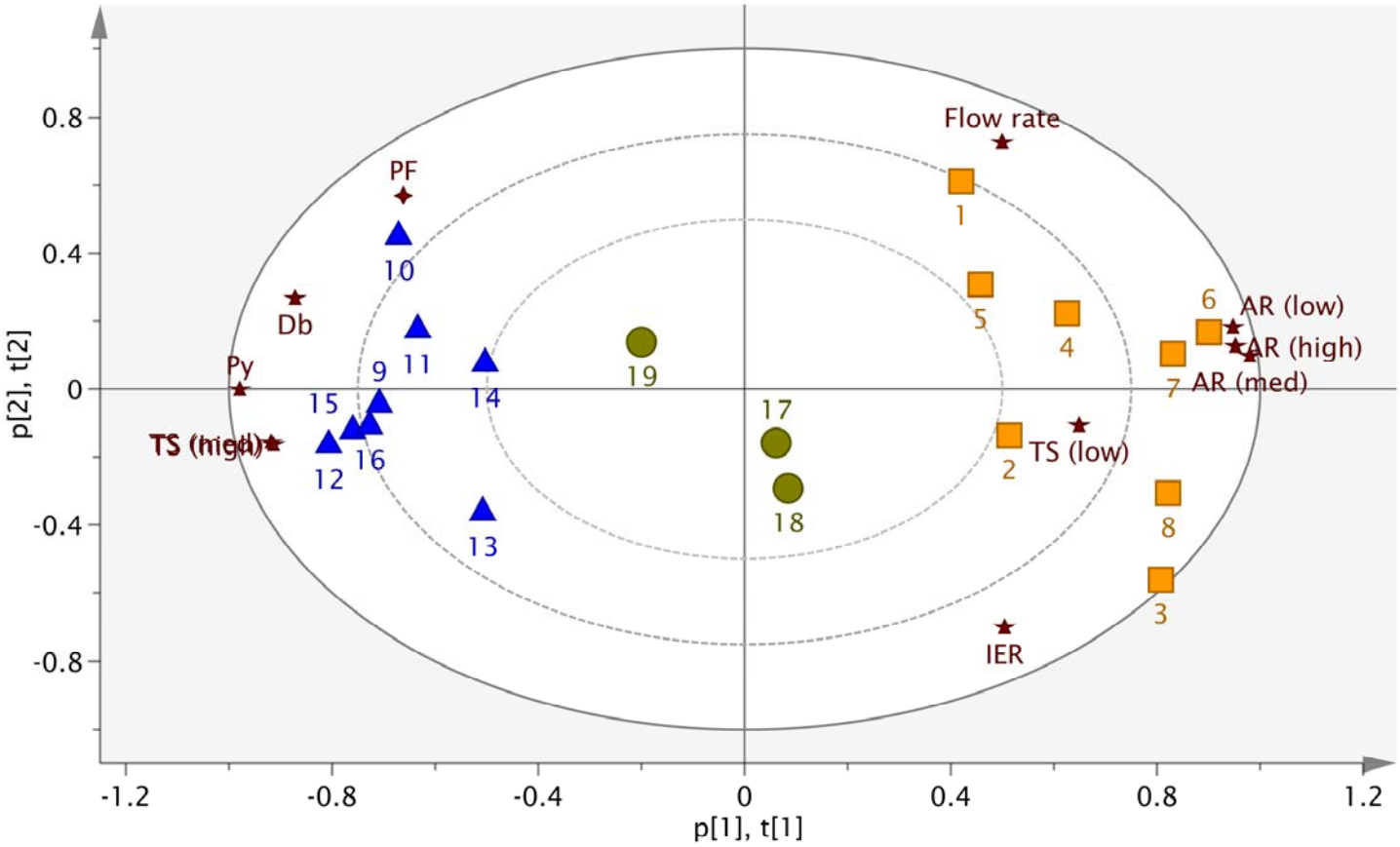

Table 1. Overview of factor setting from the experimental design.

Table 2. Evaluation of the HME-process, extrudate and tablet properties from the experimental design.

Table 3. Validation parameters of the Raman PLS model: trueness and precision indicating the accuracy of the method.

Table 4. Quantification of the CEL concentration (%) in extrudate powders of the correlating experiment (DOE) based on the PLS model with an RMSEP of 1,84 %.

Table 1. Overview of factor settings of the experimental design.

Run	Barrel T (°C)	Screw speed (rpm)	Throughput (kg/h)	Drug load (%)
1	160	50	0.2	0
2	200	50	0.2	0
3	160	200	0.2	0
4	200	200	0.2	0
5	160	50	0.5	0
6	200	50	0.5	0
7	160	200	0.5	0
8	200	200	0.5	0
9	160	50	0.2	20
10	200	50	0.2	20
11	160	200	0.2	20
12	200	200	0.2	20
13	160	50	0.5	20
14	200	50	0.5	20
15	160	200	0.5	20
16	200	200	0.5	20
17	180	125	0.35	10
18	180	125	0.35	10
19	180	125	0.35	10

Table 2. Evaluation of the HME-process, extrudate and tablet properties from the experimental design.

Run	HME-process		Extrudate properties				Tablet properties			
	Torque (%)	SME (kWh/kg)	T_g (°C)	d_{90} (μm)	Moisture (%)	True density (g/ml)	TS_{255} (MPa)	OER (%)	PF (%)	Py (MPa)
1	48.5	0.18	60.8	64.3	2.08	1.183	3.26	14.6	91.0	60.8
2	54.0	0.08	60.8	58.0	2.15	1.181	3.52	14.5	89.7	60.3
3	42.5	0.63	58.5	50.8	2.05	1.181	3.56	14.6	88.8	54.4
4	49.0	0.29	59.7	46.8	1.99	1.182	3.71	15.2	90.2	55.8
5	26.5	0.04	57.8	78.9	2.14	1.179	3.62	15.4	91.0	62.4
6	17.0	0.10	57.6	57.7	1.99	1.183	3.84	14.7	90.9	53.0
7	12.5	0.05	58.7	64.8	2.18	1.186	3.62	16.0	90.3	55.6
8	23.0	0.34	55.1	54.5	2.19	1.178	3.61	15.1	89.7	54.9
9	23.5	0.09	56.9	114.3	1.86	1.215	4.67	10.4	91.6	73.0
10	21.0	0.31	52.5	105.9	1.89	1.220	4.50	11.9	92.0	74.0
11	29.0	0.04	54.1	108.8	2.05	1.221	4.42	11.3	91.6	74.5
12	20.5	0.12	56.0	96.6	1.95	1.219	4.71	10.4	90.9	73.1
13	6.5	0.02	55.9	102.9	1.37	1.220	4.50	11.5	90.1	75.7
14	9.0	0.01	57.5	101.7	1.65	1.219	4.36	12.2	91.4	73.1
15	9.0	0.13	57.0	96.0	1.51	1.220	4.59	11.3	91.9	76.4
16	11.5	0.07	58.3	97.3	1.58	1.220	4.45	11.3	90.9	78.0
17	19.0	0.10	57.8	68.2	2.01	1.200	3.89	13.5	90.8	67.9
18	17.5	0.09	56.5	85.3	2.11	1.200	4.09	12.1	90.9	63.7
19	18.0	0.10	60.6	68.3	2.05	1.197	4.08	12.5	91.7	69.9

Table 3. Validation parameters of the Raman PLS model: trueness and precision reflecting the accuracy of the quantification method.

Validation CEL concentration (%)	Accuracy	
	Trueness (% Relative bias)	Precision (% RSD)
19.0	-7.74	0.11
20.0	-8.14	0.99
21.0	-5.62	0.37
25.0	-7.14	0.21
35.0	-6.19	0.30

Table 4. Quantification of the CEL concentration (%) in the milled extrudates of the corresponding DOE experiment based on the PLS model with an RMSEP of 1.84 %.

	Exp. N^0	**Conc. CEL (%)**
20 % CEL (label claim)	Exp. 9	19.2
	Exp. 10	20.3
	Exp. 11	20.3
	Exp. 12	20.0
	Exp. 13	19.2
	Exp. 14	19.4
	Exp. 15	19.6
	Exp. 16	19.8
10 % CEL (label claim)	Exp. 17	9.6
	Exp. 18	9.8
	Exp. 19	9.7